REGULAR PAPER

Estimation of aggregate size of red blood cell by introducing reference power spectrum measured for hemispherical ultrafine wire

Japanese Journal of Applied Physics **61**, SG1046 (2022) **REGULAR PAPER**
https://doi.org/**10.35848/1347-4065/ac4683**

Estimation of aggregate size of red blood cell by introducing reference power spectrum measured for hemispherical ultrafine wire

Kyohei Higashiyama[1], Shohei Mori[2], Mototaka Arakawa[1,2*], Satoshi Yashiro[3], Yasushi Ishigaki[3], and Hiroshi Kanai[1,2]

[1]*Graduate School of Biomedical Engineering, Tohoku University, Sendai 980-8579, Japan*
[2]*Graduate School of Engineering, Tohoku University, Sendai 980-8579, Japan*
[3]*Division of Diabetes, Metabolism and Endocrinology, Department of Internal Medicine, Iwate Medical University, Yahaba, Iwate 028-3695, Japan*

[*]E-mail: arakawa@ecei.tohoku.ac.jp

Received November 2, 2021; revised December 16, 2021; accepted December 26, 2021; published online May 30, 2022

Noninvasive measurement of the degree of red blood cell (RBC) aggregation is useful for evaluating blood properties. In the present paper, we proposed a method to estimate the size of RBC aggregates without using the power spectrum of the posterior wall by introducing a reference scattering spectrum. The reference power spectra were calculated using the power spectrum measured for an ultrafine wire with a hemispherical tip. They were applied to the size estimation of microparticles simulating RBC aggregates. The estimated sizes were close to the true values, which shows that the calculated reference power spectra were suitable for accurate size estimation. The proposed method was also applied to in vivo measurements, and the estimated sizes between at rest and in RBCs aggregated by avascularization were successfully differentiated. This demonstrates that the proposed method will be useful for estimating the size of RBC aggregates.

1. Introduction

Red blood cells (RBCs) in blood adhere to each other at a low shear rate.[1–3)] This reversible phenomenon is called RBC aggregation. RBC aggregation in plasma is enhanced by factors such as increased levels of macromolecular compounds (fibrinogen and macroglobulin) in the blood. Excessive RBC aggregation is frequently observed in diseases such as type II diabetes, deep vein thrombosis, and sepsis,[4–6)] and is thought to interfere with vasomotor tone, leading to the progression of high blood pressure. It may negatively affect the microcirculation and nutrient supply.[7,8)] The increase in RBC aggregation is known to increase the blood viscosity in large vessels, such as veins in the lower extremities with low shear force,[6,9)] and it is an indicator highly related to blood properties. Therefore, the evaluation of RBC aggregation is clinically meaningful for the evaluation of blood properties as well as the screening of these diseases.

Increased RBC aggregation can be observed as the increased brightness of the vessel lumen (smoke-like echo) on ultrasound B-mode images.[10,11)] Although the evaluation of blood properties based on the smoke-like echo is useful, it is qualitative.[12,13)]

There are several studies on the quantitative evaluation of RBC aggregation using ultrasound. Shung et al. observed changes in the brightness of porcine blood echoes during a cardiac cycle,[14,15)] and Patat et al. observed the changes in the sound velocity and the scatterer size during blood coagulation using human whole blood *in vitro*.[16,17)] All of these evaluation methods were applied to the blood drawn by blood sampling; therefore, they were invasive.

The evaluation of ultrasound backscattering characteristics is a quantitative method for tissue characterization. By estimating the backscatter coefficient and the attenuation coefficient of the tissue based on the frequency spectrum of the radiofrequency (RF) signal obtained from the object, the structural parameters, such as, the shape, size, and concentration can be estimated. This method has been applied for the analysis and classification of various tissues, such as, the liver, skin, lymph nodes, and blood.[18–27)]

Cloutier et al. calculated the backscattering coefficient from the RF signal obtained from the vascular lumen and estimated the attenuation coefficient of tissues and the parameters indicating the structure of the RBC aggregates,[24–26)] and showed the possibility of monitoring the systemic inflammatory state by in vivo measurements.[27)] However, few studies using these methods have involved human subjects, and diagnosis using this method has not been clinically established.

We have studied a noninvasive and quantitative method for measuring blood properties.[28–37)] Saito et al. assumed that RBCs aggregate as a single-sphere scatterer and estimated the size from the scattering characteristics extracted by normalizing the power spectrum measured from the vessel lumen with that from the rear wall using a focused ultrasound transducer.[28–32)] We also examined the relationship between RBC aggregation using ultrasound and blood glucose level. Sakaki et al. compared the blood glucose levels with the parameters determined from changes in the scattering power spectra of the echoes from the vascular lumen before and after avascularization.[33,34)] Fukase et al. studied the relationship between the blood glucose levels and the brightness values of the B-mode image.[35)] However, there are still problems, such as the low correlation between these parameters and the blood glucose levels and the lack of reproducibility of the results because of the variation in the data among the measurements. The development of a more accurate method for evaluating the degree of RBC aggregation would solve these problems.

In our estimation method of the RBC aggregate size, we regarded the rear wall of the vessel as the reflector, and the reflection property at the rear wall was assumed to be independent of frequency. However, because high-frequency ultrasound with a center frequency of approximately 40 MHz was used, the reflection characteristics of the rear wall might have frequency dependence owing to the surface roughness and the slope of the vessel wall to the probe surface. This causes errors in the size estimation results.

Moreover, Fukase et al. suggested that the effect of elevational misalignment of vessels in the long-axis measurement on the evaluation of the degree of RBC aggregation

could be reduced by short-axis measurement.[36] However, in the short-axis measurement of the vessel, few beams can be used as the signal of the rear wall, making it difficult to remove the dips that appear on the averaged power spectrum. Therefore, robust size estimation using short-axis measurements could be difficult.

To directly estimate the size of the RBC aggregates using only the scattering power spectrum obtained from the vascular lumen, we measured the power spectra for the three wires with a hemispherical edge assumed to be a single-sphere scatterer to calculate the reference scattering power spectra. Subsequently, the ratios of the power spectra measured for the two wires with different diameters were calculated using three combinations. The ratios were compared with those of the theoretical scattering power spectra corresponding to the diameters of the wires to evaluate the accuracy of the reference power spectra.[37] In the present paper, we estimated the size of the microparticles with different diameters to evaluate the accuracy of the proposed size estimation method using the reference scattering power spectrum. Moreover, we investigated the clinical usefulness of our method by estimating the size of RBC aggregates in the dorsal hand vein.

2. Principle and methods

2.1. Calculation of the reference power spectra

In the present paper, the RBC aggregate was assumed to be a single-sphere scatterer with numerous point sources on the surface. The theoretical power spectrum obtained by irradiating a plane wave is expressed as

$$\frac{Q(ka)}{4\pi a^2} = \sum_{n=0}^{\infty} \frac{2n+1}{(ka)^2} \sin^2[\delta_n'(ka)], \tag{1}$$

where $Q(ka)$ is the scattering cross section, k is the wavenumber, a is the radius of the scatterer, n is the number of point sources on the surface of the scatterer, and $\delta_n'(ka)$ is the derivative of the phase difference between the incident and scattered waves.[38] Figure 1(a) shows the power spectra calculated using Eq. (1) for scatterer sizes of 2–60 μm. Here, the biological sound speed ($c = 1540\ \mathrm{m\ s^{-1}}$) was assumed, and the wavenumber k was converted to frequency f using the relation $f = ck/2\pi$. As shown in Fig. 1(a), the slope of the power spectrum decreased as the scatter size increased. The size of the RBC aggregate was estimated using the inclination differences in the frequency dependence among the scatterer sizes.

In the present paper, the scattering power spectrum $P_s(f, d)$ was obtained by measuring the vascular lumen at a depth d. $P_s(f, d)$ includes not only the scattering property $S(f)$ but also the frequency dependence of the applied signal $X(f)$, transmission and reception properties of the ultrasonic transducer $G(f)$, sound pressure property of the ultrasound probe at depth d, $H(f, d)$, and attenuation property $A(f, d)$. Therefore, the scattering power spectrum $P_s(f, d)$ from the vascular lumen at depth d is given by:

$$P_s(f, d) = |S(f)X(f)G(f)H(f, d)A(f, d)|^2. \tag{2}$$

Thus, the reference power spectrum $P_{RD}(f, d)$ for the comparison with $P_s(f, d)$ is given by

$$P_{RD}(f, d) = |S_D(f)X(f)G(f)H(f, d)A(f, d)|^2, \tag{3}$$

where $S_D(f)$ is the theoretical scattering property of a single sphere with diameter of D. In the present paper, the reference power spectrum $P_{RD}(f, d)$ was calculated by measuring the ultrafine wire with a hemispherical tip. Let us define the power spectrum $P_\phi(f, d)$ obtained from the ultrafine wire at depth d in water as

$$P_\phi(f, d) = |S_\phi(f)X(f)G(f)H(f, d)A_w(f, d)|^2, \tag{4}$$

where $A_w(f, d)$ is the attenuation property of the water. The reference scattering power spectrum $P_{RD}(f, d)$ with an arbitrary diameter D is obtained by the product of $P_\phi(f, d)$ and the ratio $|S_D(f)|^2/|S_\phi(f)|^2$ of the theoretical power to the power of the wire, as follows:

$$P_{RD}(f, d) = P_\phi(f, d) \times \left| \frac{S_D(f)}{S_\phi(f)} \right|^2. \tag{5}$$

2.2. Estimation of the size of RBC aggregates

Wires in water were used as the targets to obtain the reference power spectrum. Ultrasound propagates in the skin and blood

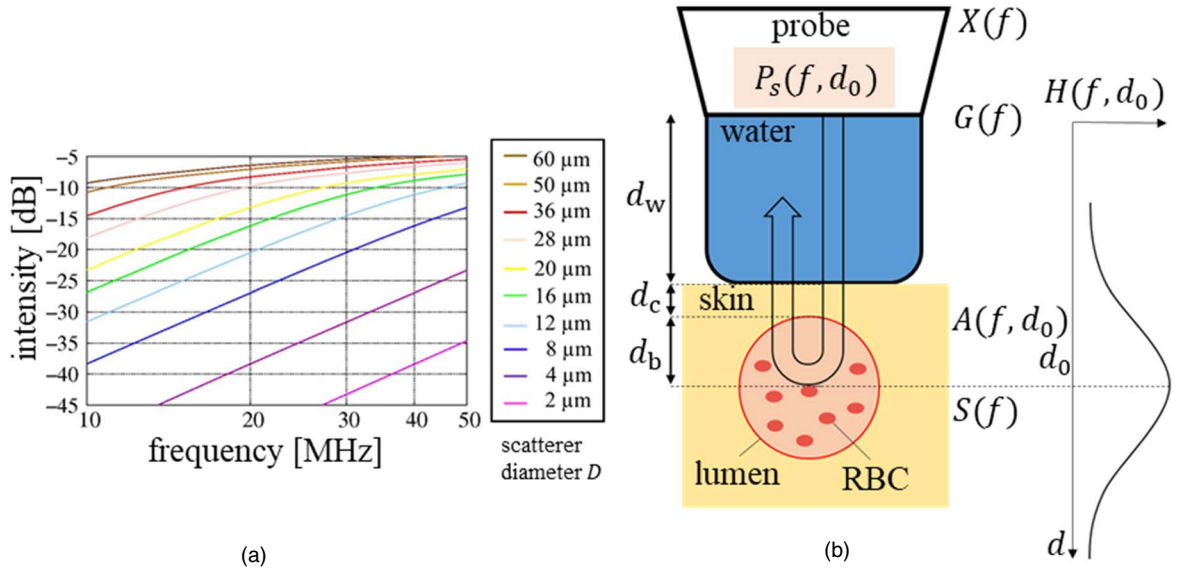

(a) (b)

Fig. 1. (Color online) (a) Theoretical scattering power spectra $10\log_{10}\{Q(ka)/4\pi a^2\}$ and (b) the schematic diagram of the in vivo measurement.

after propagation in the water in the membrane attached to the probe in vivo. Therefore, it is inappropriate to directly fit the measured power spectrum to the calculated reference scattering power spectra because there is an attenuation characteristic difference owing to the different propagation paths of the two measurements. The correction component $C_s(f, d)$ which shows the difference in propagation attenuation characteristics between in vivo and wire measurements, was calculated using the propagation path of the skin d_c, that of the blood d_b, and the attenuation coefficient of the skin $\alpha_c(f)$, that of the blood $\alpha_b(f)$, and that of the water $\alpha_w(f)$ as follows:

$$C_s(f, d) = 2d_c\alpha_c(f) + 2d_b\alpha_b(f) - 2(d_c + d_b)\alpha_w(f). \tag{6}$$

The first and second terms on the right-hand side of Eq. (6) shows the propagation attenuation in the in vivo measurement, and the third term shows that in the measurement of the wire.

The attenuation coefficient of the skin $\alpha_c(f)$ was calculated by correcting the difference in the sound pressure properties for the difference in the power spectra measured at the different depths d_1 and d_2 in the target.[32] The ratio of the measured power spectra $P_c(f, d_1)$ and $P_c(f, d_2)$ at different depths d_1 and d_2, respectively, by setting the focal point at a depth of $d_0 = d_w + d_c/2$ in Fig. 1(b) corresponds to the sum of the difference in the attenuation properties $|A_c(f, d_1)|^2/|A_c(f, d_2)|^2$ and difference in the sound pressure properties $|H(f, d_1)|^2/|H(f, d_2)|^2$ are as follows:

$$\begin{aligned} &10\log_{10}\frac{P_c(f, d_1)}{P_c(f, d_2)} \\ &= 10\log_{10}\frac{|S_c(f)A_w(f, d_w)A_c(f, d_1 - d_w)H(f, d_1)G(f)X(f)|^2}{|S_c(f)A_w(f, d_w)A_c(f, d_2 - d_w)H(f, d_2)G(f)X(f)|^2} \\ &= 10\log_{10}\frac{|A_c(f, d_1 - d_w)|^2}{|A_c(f, d_2 - d_w)|^2} + 10\log_{10}\frac{|H(f, d_1)|^2}{|H(f, d_2)|^2}, \end{aligned} \tag{7}$$

where, $S_c(f)$ is the scattering characteristics of the skin. Subsequently, the attenuation property $|A(f, d)|$ is expressed using the attenuation coefficient $\alpha(f)$ as:

$$|A(f, d)| = e^{-2d\times\frac{\alpha(f)}{8.686}}, \tag{8}$$

where, e is the base of the natural logarithm, and $10\log_{10}e^2 = 8.686$. From Eqs. (7) and (8), the attenuation coefficient $\alpha_c(f)$ can be expressed as follows:

$$\alpha_c(f) = \frac{1}{2(d_2 - d_1)}\left\{10\log_{10}\frac{P_c(f, d_1)}{P_c(f, d_2)} - 10\log_{10}\frac{|H(f, d_1)|^2}{|H(f, d_2)|^2}\right\}[\text{dB mm}^{-1}]. \tag{9}$$

The difference in the sound pressure properties is acquired in advance by the measurements for a reflector set at different depths in water. The ratio of the power spectra $P_r(f, d_1)$ and $P_r(f, d_2)$ for the reflector measured at different depths d_1 and d_2, respectively, corresponds to the sum of the difference in sound pressure properties $|H(f, d_1)|^2/|H(f, d_2)|^2$ and the difference in the attenuation properties of water $|A_w(f, d_1)|^2/|A_w(f, d_2)|^2$ as follows:

$$\begin{aligned} &10\log_{10}\frac{P_r(f, d_1)}{P_r(f, d_2)} \\ &= 10\log_{10}\frac{|R_0A_w(f, d_1)H(f, d_1)G(f)X(f)|^2}{|R_0A_w(f, d_2)H(f, d_2)G(f)X(f)|^2} \\ &= 10\log_{10}\frac{|H(f, d_1)|^2}{|H(f, d_2)|^2} + 10\log_{10}\frac{|A_w(f, d_1)|^2}{|A_w(f, d_2)|^2}, \end{aligned} \tag{10}$$

where, R_0 is the reflectance property of the reflector. By solving Eq. (10) for $10\log_{10}|H(f, d_1)|^2/|H(f, d_2)|^2$, the difference in the sound pressure properties can be obtained as follows:

$$\begin{aligned} 10\log_{10}\frac{|H(f, d_1)|^2}{|H(f, d_2)|^2} &= 10\log_{10}\frac{P_r(f, d_1)}{P_r(f, d_2)} \\ &- 10\log_{10}\frac{|A_w(f, d_1)|^2}{|A_w(f, d_2)|^2}. \end{aligned} \tag{11}$$

The difference in the attenuation properties of water $|A_w(f, d_1)|^2/|A_w(f, d_2)|^2$ can be calculated from Eq. (8) using the attenuation coefficient of water $\alpha_w(f)$.[39] The attenuation coefficient $\alpha_c(f)$ can be calculated by substituting $|H(f, d_1)|^2/|H(f, d_2)|^2$ in Eq. (9). In addition, the attenuation coefficient of blood $\alpha_b(f)$ is calculated using the same procedure by setting the focal point at the center of the vascular lumen. That is, $P_s(f, d_1)$ and $P_s(f, d_2)$ are calculated by changing the analysis window positions for the measured signal to obtain the power spectrum measured from the vascular lumen $P_s(f, d)$.

After correcting the power spectrum measured from the vascular lumen $P_s(f, d)$ by multiplying the calculated correction term $C_s(f, d)$, the corrected power spectrum $P_s'(f, d)$ and the reference scattering power spectra were fitted using the weighted least-squares method, as shown in Eq. (12). Thereafter, the size of the RBC aggregate was estimated by minimizing the following error ΔP_D.

$$\begin{aligned} \Delta P_D = \sum_{k=0}^{N-1} w(f_k)[&10\log_{10}P_s'(f_k, d) \\ &- 10\log_{10}P_{RD}(f_k, d) + b\,]^2, \end{aligned} \tag{12}$$

where b is the intercept of the theoretical spectrum and $w(f_k)$ is the weighting function defined to use a reliable frequency range for the fitting and is calculated by dividing the power spectrum in water without the object from the obtained scattered power spectrum $P_s(f, d)$.

2.3. Experiment

2.3.1. Measurement for the ultrafine wires. An ultrafine wire with a hemispherical tip was set parallel to the beam direction (z-axis direction) of the ultrasonic probe for the ultrasound measurement, as shown in Fig. 2(a), where d_w is the propagation path length of water. Figure 2(b) shows a micrograph of the wire (diameter $\phi = 40$ μm). An ultrasound system (Tomey UD-8000) was used. The sampling frequency was 240 MHz. A mechanical scanning linear probe with an operating center frequency of 30 MHz (frequency range: 19–40 MHz) was used. The focal length of the probe, this is composed of a concave transducer and a mechanical scanner, was 8.75 mm, and the distance between the ultrasonic transducer and the tip of the wire d_0 was set to 8.75 mm.

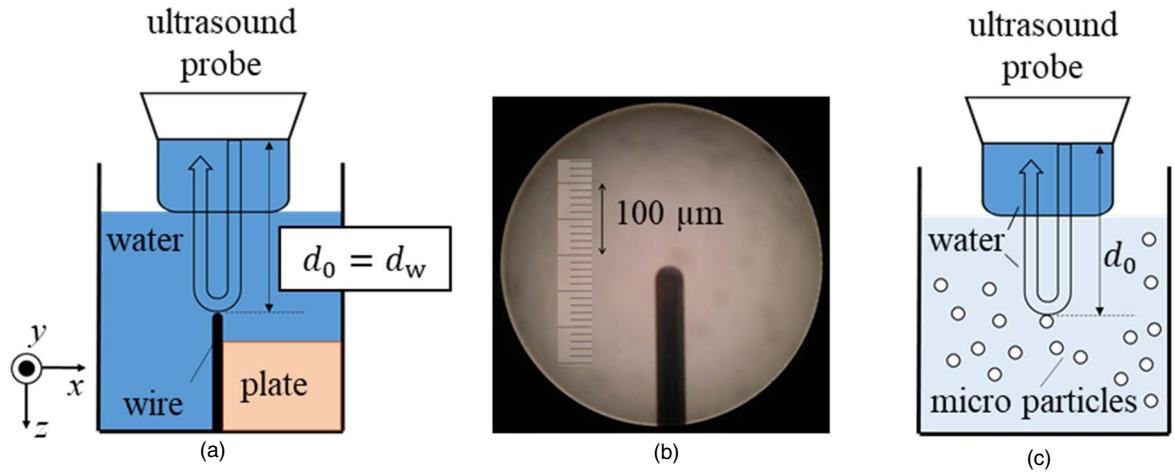

Fig. 2. (Color online) (a) Schematic diagram of the wire measurement, (b) micrograph of a wire ($\phi = 40\,\mu$m), and (c) schematic diagram of the phantom measurement.

Ultrafine wires with diameters $\{\phi\}$ of 20, 30, and 40 μm were used. To accurately align the measurement position of the tip of the wire, the mechanical scanning of the ultrasound probe was stopped and it was manually moved with a 2 μm step in each of the x-axis and y-axis directions to obtain the largest amplitude of the signal from the tip of the wire. The power spectrum $P_\phi(f, d_0)$ was calculated by windowing the RF signal with a rectangular window with a width of 0.2 μs.

In addition, when the accurate scattering property $S(f)$ is included in the calculated power spectrum $P_\phi(f, d_0)$, the ratio of the scattering power spectra obtained from single-sphere scatterers with different diameters ϕ_1 and ϕ_2 agree with that of the theoretical powers with diameters ϕ_1 and ϕ_2, as

$$\frac{P_{\phi_1}(f,d)}{P_{\phi_2}(f,d)} = \left| \frac{S_{\phi_1}(f)G(f)X(f)H(f,d)A(f,d)}{S_{\phi_2}(f)G(f)X(f)H(f,d)A(f,d)} \right|^2 = \left| \frac{S_{\phi_1}(f)}{S_{\phi_2}(f)} \right|^2. \quad (13)$$

This relationship was used to evaluate the accuracy of the scattering characteristics included in the power spectrum $P_\phi(f, d_0)$ measured for the wire.

2.3.2. Phantom experiment. To evaluate the accuracy of the proposed size estimation method, the sizes of the microparticles simulating RBC aggregates were estimated using reference power spectra. Based on Eq. (5), the reference power spectra $P_{RD}(f, d_0)$ were calculated with a 1 μm step in the range of $D =$ 2–60 μm using the power spectrum $P_{20}(f, d_0)$ obtained from the wire with a diameter of 20 μm. Blood-simulating phantoms were prepared by suspending microparticles with diameters of 5 and 20 μm in water. Accurate measurements are difficult for microparticles with high volume ratios because of the large attenuation owing to the large difference in acoustic impedances between the particles and water. Thus, the volume ratio of the particles was set to 1%.

The experimental system for the B-mode is shown in Fig. 2(c). The number of beams was 113, and 20 frames were acquired. The scattering power spectrum was calculated by windowing the acquired RF signal with a Hanning window of width 0.15 μs centered at a depth of $d_0 = 8.75$ mm. The power spectrum for the size estimation, $P_m(f, d_0)$, was calculated by averaging the scattering power spectra with 113 beams. The term to compensate for the difference in the attenuation properties between the wire measurement and phantom measurement, $C_m(f, d)$, is given by:

$$C_m(f, d) = 2d_m\{\alpha_m(f) - \alpha_w(f)\}, \quad (14)$$

where d_m is the propagation path length of the blood-simulating phantom, and $\alpha_m(f)$ is the attenuation coefficient of the phantom. $\alpha_m(f)$was calculated from the power spectra of phantom calculated as the depths of $d_1 = 8.2$ mm and $d_2 = 9.0$ mm by correcting the sound pressure characteristics difference.[32] The literature value was used as the attenuation coefficient of water $\alpha_w(f)$.[39] The corrected power spectrum $P'_m(f, d_0)$ was obtained by multiplying the correction term $C_m(f, d)$ to $P_m(f, d_0)$ for each frame, and the size of the microparticles was estimated by fitting the corrected power spectrum $P'_m(f, d_0)$ with the reference scattering power spectra $P_{RD}(f, d_0)$.

2.3.3. In vivo measurement. The size of the RBC aggregate was estimated by in vivo measurements for a healthy subject in their 20 s. First, to calculate the attenuation coefficient of the skin, $\alpha_c(f)$, the RF signal was measured from the skin by long-axis measurement by setting the focal point at a depth of $d_0 = d_w + d_c/2$. The power spectra were calculated by windowing the RF signal with the Hanning window at the depths of $d_1 = 8.2$ mm and $d_2 = 9.0$ mm, and the attenuation coefficient of the skin, $\alpha_c(f)$, was determined. Next, the RF signal was obtained from the vascular lumen using ultrasonic short-axis measurements. The focal point was set as the center of the lumen of the dorsal hand vein, as shown in Fig. 3(a). RBC aggregation is more likely to occur under low-shear-rate conditions. Therefore, in addition to the measurements at rest, the RF signals were measured under the condition of avascularization using crucible scissors.[35] The blood flow was stopped by pressing two points on the fingertip side and the heart side of the vein, as shown in Fig. 3(b), to prevent the backflow of the blood. Five frames were obtained every 10 s for 0–190 s, and the blood flow was stopped from 60 to 190 s. Fifteen beams (± 7 beams for the beam passing through the center of the vascular lumen) were used in each frame. The power spectra calculated by windowing the signals with a Hanning window

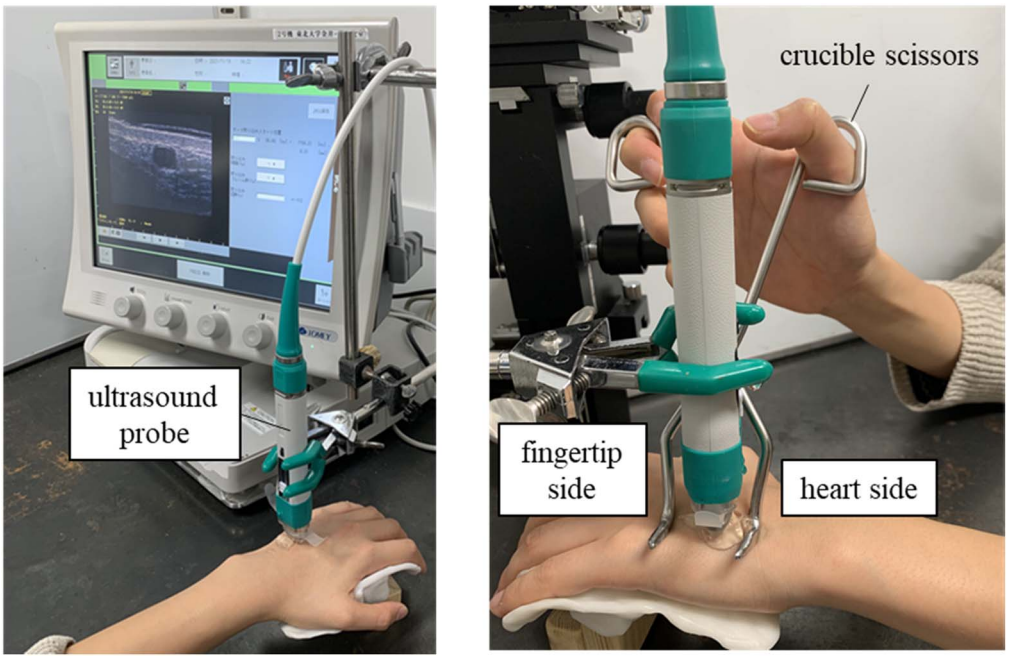

Fig. 3. (Color online) (a) State of in vivo measurement and (b) state of avascularization.

with a width of 0.15 μs at the focal point of the ultrasound probe were averaged with 15 beams for 5 frames to obtain the power spectrum $P_s(f, d_0)$ at each time.

The attenuation measurements for the skin, d_1 and d_2, were set to calculate the power spectra from the blood, and the attenuation coefficient $\alpha_b(f)$ of the blood at each time point was calculated. The correction terms $C_s(f, d_0)$ calculated using $\alpha_c(f)$ and $\alpha_b(f)$ in Eq. (6) was multiplied by the power spectrum $P_s(f, d_0)$, and the size of the RBC aggregate was determined by fitting the corrected power spectrum and the reference scattering power spectra. Because the blood vessel moves significantly immediately after avascularization and the aggregation state is not stable owing to the influence of the shear rate immediately before the avascularization,[27] the estimated sizes at rest (0–60 s) and that at the latter 7 frames (130–190 s) during avascularization were compared.

Moreover, to evaluate the usefulness of the proposed method, the size of the RBC aggregates was estimated using the conventional method.[32] The scattering characteristics were obtained by normalizing the power spectrum of the vascular lumen $P_s(f, d_0)$ with that of the posterior wall. The RBC aggregate sizes were estimated by fitting the normalized power spectrum to the theoretical power spectrum. Afterwards, the estimated sizes were compared with those estimated using the proposed method.

3. Results and discussion

3.1. Measurement for the wire

Figure 4(a) shows the power spectra $P_\phi(f, d_0)$ measured for each of the hemispherical ultrafine wires with different diameters $\{\phi\}$. The figure shows that the power increased with a larger diameter. Figure 4(b) shows the ratios of the power spectra $P_\phi(f, d_0)$ obtained from the wires with different diameters $\{\phi\}$ and the ratios of the theoretical scattering powers $|S_\phi(f)|^2$ for the corresponding diameters of the wires. In Figs. 4(b-1), 4(b-2), and 4(b-3), the averages and the standard deviations of the differences $\{\varepsilon(f)\}$ between them were calculated in the 6 dB-band as

$$\varepsilon(f) = 10\log_{10}\frac{P_{\phi_1}(f,d_0)}{P_{\phi_2}(f,d_0)} - 10\log_{10}\left|\frac{S_{\phi_1}(f)}{S_{\phi_2}(f)}\right|^2. \quad (15)$$

The averaged differences (the standard deviations) were 1.3 (0.51), 5.6 (0.38), and 7.5 (0.76) dB for Figs. 4(b-1), 4(b-2), and 4(b-3), respectively. The standard deviations were less than 1 dB in all cases, although the average differences were relatively large for Figs. 4(b-2) and 3(b-3). Thus, the power ratio of the measured power spectra for the wires and the theoretical scattering power ratio showed similar frequency characteristics.

The frequency characteristics of Figs. 4(b-2) and 4(b-3) were similar to those of the theoretical power ratio, but the averages of the differences $\{\varepsilon(f)\}$ were larger than those in Fig. 4(b-1). This is caused by the effect of the sound pressure distribution of the transmitted wave. In the present paper, the transmitted wave was assumed to be a plane wave, although the focused wave was transmitted. Thus, the sound pressure is distributed in the lateral direction near the focus. Figure 4(c) shows the measured amplitude distribution of the ultrasound probe for a wire with a diameter of 30 μm by moving the ultrasound probe in 2 μm steps in the direction of the x-axis in Fig. 2(a). This shows that the sound field distribution became flatter as it got away from the focal point and approached the characteristics of a plane wave.

Figure 4(d) shows the averaged differences between the power ratio of the measured power spectra for the wire in the case of $d_0 = 8.75$ and 9.0 mm and the theoretical scattering power ratio. The average differences at $d_0 = 9.0$ mm became smaller compared to those at $d_0 = 8.75$ mm. Thus, the sound pressure distribution became smaller at points farther from the focal point. Because the measurement target was spherical, the phase of the scattered wave differed at each lateral position. The components having phases that cancel the

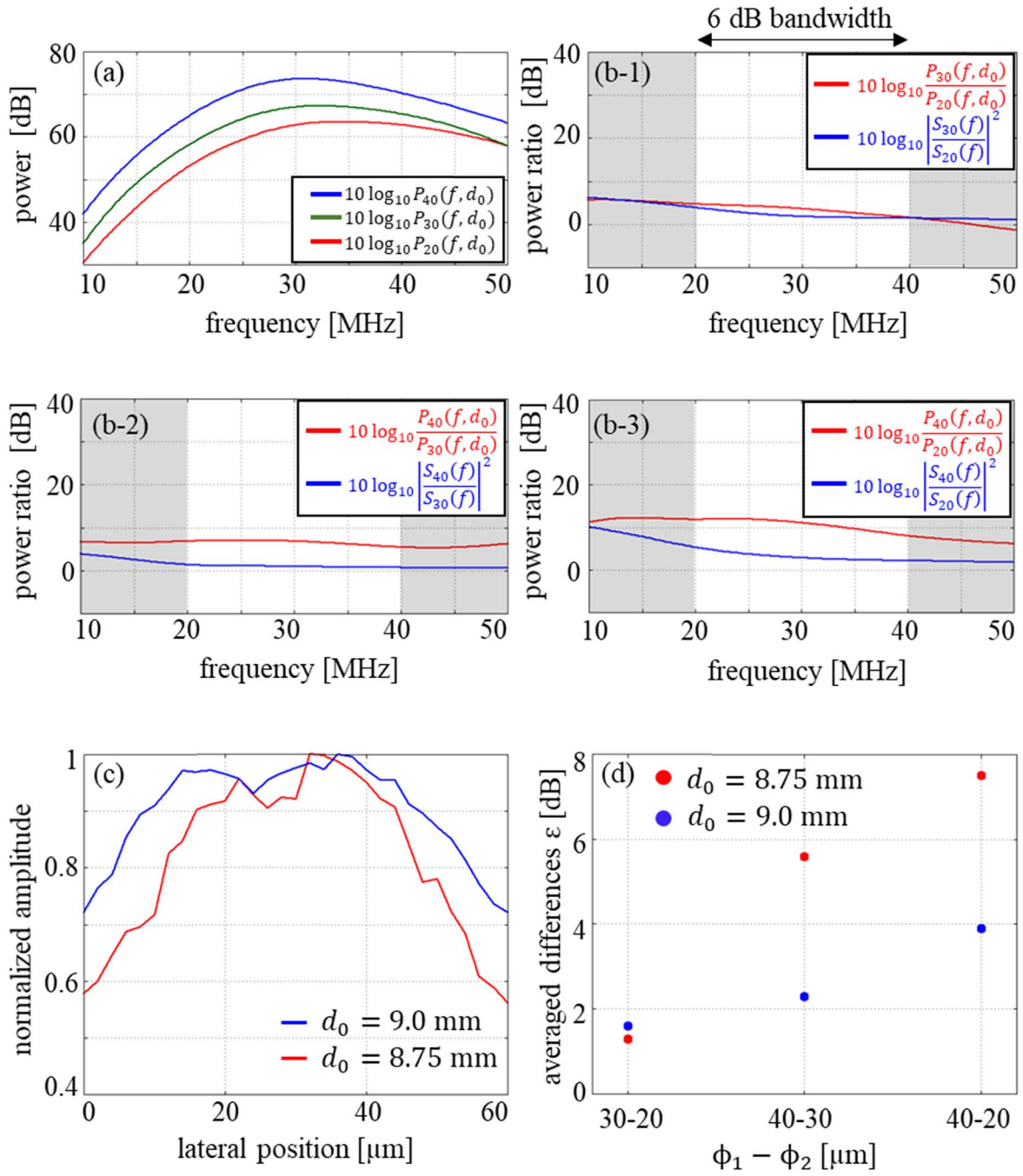

Fig. 4. (Color online) (a) The power spectra for the wires, (b) the ratio of the power spectra $\{P_{\phi_i}(f, d_0)\}$ from the wires with different diameters $\{\phi_i\}$ and theoretical power ratio corresponding to the diameters of the wires, (b-1) $\phi_1 = 30$ μm, $\phi_2 = 20$ μm, (b-2) $\phi_1 = 40$ μm, $\phi_2 = 30$ μm, (b-3) $\phi_1 = 40$ μm, $\phi_2 = 20$ μm, (c) the results of the sound field measurements, and (d) the average of the differences $\varepsilon(f)$ due to change in d_0.

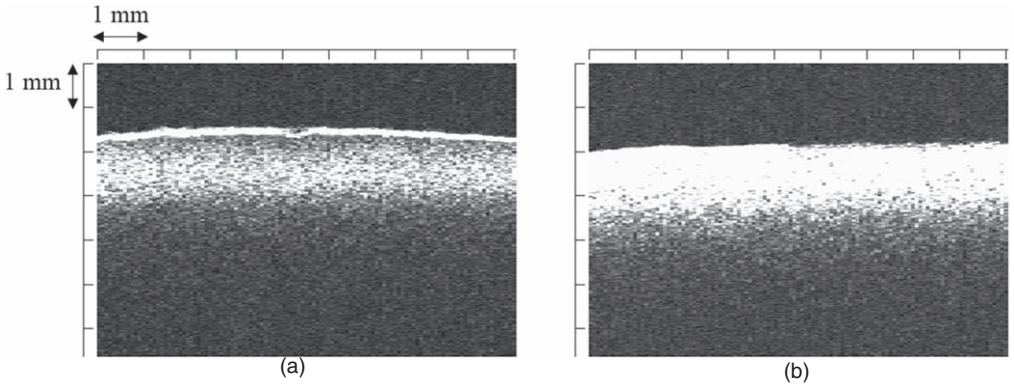

Fig. 5. B-mode images of the blood-simulating phantoms. (a) 5 μm and (b) 20 μm.

backscattered power might decrease owing to the sound pressure distribution. This effect increases as the diameter of the wire increases, which increases the power difference between wires with different diameters. Consequently, the calculated power ratios of the wires may increase.

In the actual estimation of the RBC aggregate size, the frequency dependences between the measured power spectrum and the calculated reference scattering power spectra are fitted by changing the offset to minimize the difference, considering the difference between the ultrasonic reflectivity for water and wire and that for plasma and RBCs. Therefore, the measured spectrum $P_{\phi}(f, d_0)$ for the wire is suitable for calculating the reference scattering power spectra because the power ratio measured for the wires showed similar frequency characteristics to that of the theoretical power spectra.

3.2. Phantom experiment

B-mode images of the blood-simulating phantom are shown in Fig. 5. This shows that the image became brighter as the particle size increased. Figure 6(a) shows the averaged power spectra $\{P_{\mathrm{m}}(f, d_0)\}$ among the 20 frames with standard deviations. Figure 6(b) shows the averages and standard deviations of the calculated attenuation coefficients $\alpha_{\mathrm{m}}(f)$ of the blood-simulating phantoms over 20 frames. It shows that the calculated attenuation coefficient $\alpha_{\mathrm{m}}(f)$ was close to linear in the 6 dB bandwidth from 19 to 40 MHz, and the attenuation coefficient $\alpha_{\mathrm{m}}(f)$ increased as the particle size increased. A 6 dB bandwidth of 19–40 MHz was determined for the reflection spectrum acquired for the reflector in water. Because the backscattered power increased as the particle size increased, as shown in Fig. 5, it is a reasonable trend that the propagation attenuation also increased with the larger particle size.

The correction term $C_{\mathrm{m}}(f, d_0)$ is calculated using Eq. (14), and the size of the particle was estimated by fitting the corrected power spectrum $P'_{\mathrm{m}}(f, d_0)$ with the reference power spectra $P_{RD}(f, d_0)$. The estimated sizes are presented in Table I. This shows that the estimated sizes are close to the true sizes. The difference in the estimated sizes of the particles with different sizes was also confirmed. Figures 6(c) and 6(d) show the fitting results of the corrected power spectrum and the reference power spectrum, which corresponded to the estimated sizes of 5 μm and 20 μm particles, respectively. The root means squared errors (RMSEs) of the fitting were 0.7 dB and 0.3 dB for the particle diameters of 5 μm and 20 μm, respectively. This shows that the corrected power spectrum $P'_{\mathrm{m}}(f, d_0)$ was well fitted with the reference power spectrum. These results show that the reference scattering power spectra are useful for the accurate size estimation of scatterers.

3.3. In vivo measurement

The size of the RBC aggregates was estimated using in vivo measurements. Figure 7(a) shows the averaged values and standard deviations of the attenuation coefficient of the skin $\alpha_{\mathrm{c}}(f)$ for eight frames, which is similar to the frequency characteristics in the literature.[40)]

Next, RF signals were acquired from the vascular lumen by short-axis measurements. Figures 7(b-1) and 7(b-2) show the ultrasonic B-mode images of the vascular lumen at rest and with RBCs aggregated by avascularization, respectively.

Figure 8(a) shows the averages and standard deviations of the power spectra $P_{\mathrm{s}}(f, d_0)$ averaged over seven frames at rest and during avascularization. The attenuation coefficient $\alpha_{\mathrm{b}}(f)$ of the blood was also calculated for each frame, and

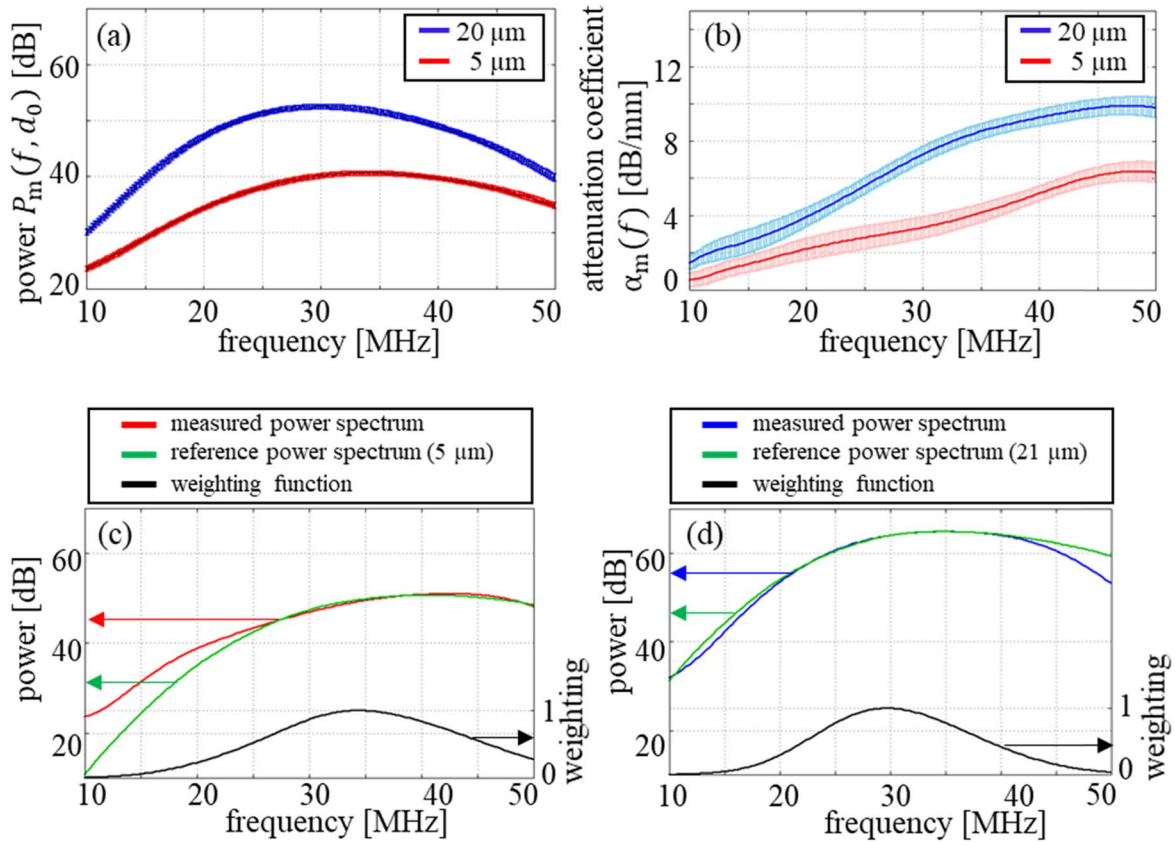

Fig. 6. (Color online) (a) The power spectra measured from the blood-simulating phantom, (b) the attenuation coefficient of the phantom, (c) the fitting result (5 μm), and (d) the fitting result (20 μm).

Table I. Estimated sizes of the microparticles.

Micro particles	5 μm	20 μm
Average [μm]	8.3	19.3
Standard deviation [μm]	3.6	2.2

the averages and standard deviations among frames at rest and during avascularization are shown in Fig. 8(b). The attenuation coefficient at rest was 2.2 dB mm^{-1} at 30 MHz, and that of the sampled blood was 1.2 dB mm^{-1} at 30 MHz in the literature.[41] It shows that the calculated $\alpha_b(f)$ was close to that of the literature. Moreover, the correction term $C_s(f, d_0)$ is calculated using Eq. (6), the power spectrum $P_s(f, d_0)$ was corrected, and the size of the RBC aggregates was estimated by fitting the corrected power spectrum $P_s'(f, d_0)$ to the reference power spectra $P_{RD}(f, d_0)$.

Table II shows the averages and standard deviations of the estimated sizes of RBCs at rest and during avascularization. In healthy subjects, RBCs do not aggregate without avascularization. The diameter of a single RBC was approximately 6–8 μm.[42,43] In the proposed method, the average estimated size at rest was 8.1 μm, which is reasonable. The average estimated size during the avascularization was 15.2 μm, which corresponds to the increase in size due to RBC aggregation. Figures 8(c) and 8(d) show the fitting results of the corrected power spectrum $P_s'(f, d_0)$ and the reference power spectrum at rest and during avascularization, respectively. The RMSEs of the fitting in Figs. 8(c) and 8(d) were 0.7 dB and 0.2 dB, respectively, which shows that the corrected power spectrum $P_s'(f, d_0)$ was well fitted with the reference power spectrum. The average of the RMSEs of the fitting among frames are shown in Table III. This shows that the fitting error in the proposed method is smaller than that in the conventional method.

In the conventional method, the average of the estimated size at rest was 25.1 μm, which was much larger than the diameter of a single RBC, and the normalized power spectrum did not fit well with the theoretical power spectrum, as shown in Fig. 9(a). The power spectra of the posterior wall might be frequency dependent due to the slope and surface shape of the posterior wall. In fact, the power spectra of the posterior wall that were used for the size estimation varied among the beams, as shown in Fig. 9(b). This probably affected the accuracy of the size estimation using the conventional method. Moreover, in this study, the short-axis scan was used for the measurement to reduce the effect of the elevational misalignment of vessels in the long-axis measurement.[36] In this measurement, the number of beams that can be used as the signals of the posterior wall is small, and the effect of the dip caused by the unwanted signals included in the analysis range of the posterior wall might not be removed. This might increase the fitting error of the conventional method.

In the proposed method, the corrected power spectrum $P_s'(f, d_0)$ fitted well with the reference power spectrum, even though the scattered waves from RBCs interfered with each other. The effect of interference might be reduced by

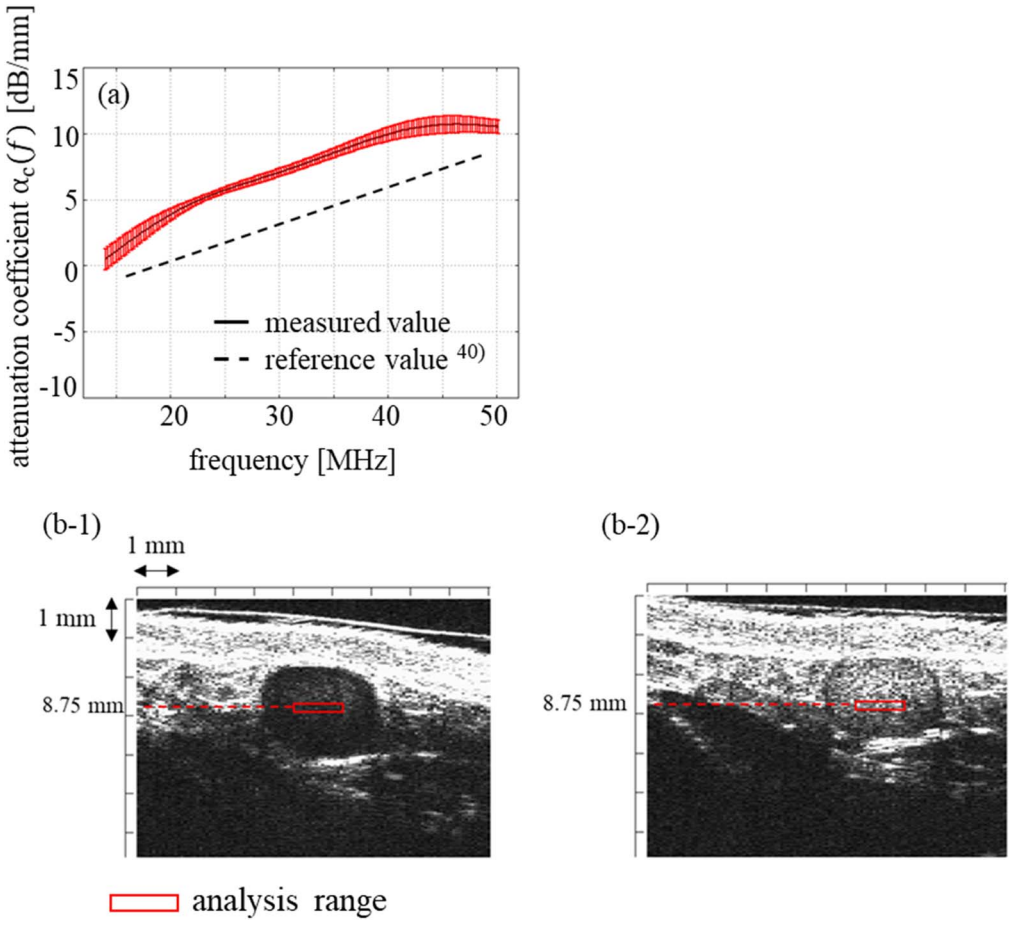

Fig. 7. (Color online) (a) The estimated attenuation coefficient of the skin, (b-1) B-mode image at rest, and (b-2) B-mode image during avascularization.

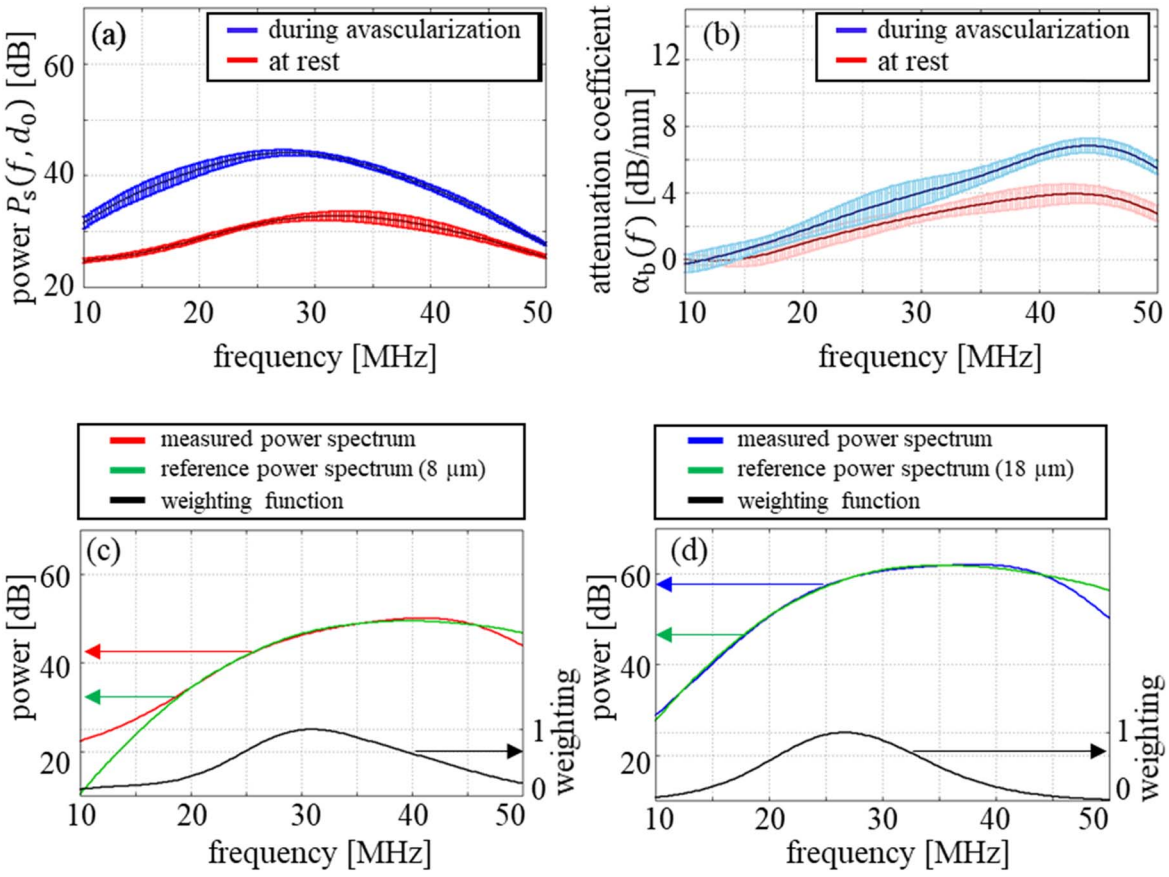

Fig. 8. (Color online) (a) The power spectra measured for the vascular lumen, (b) the attenuation coefficient of blood, (c) the fitting result at rest, and (d) the fitting result during avascularization.

Table II. Estimated sizes of RBC aggregates (unit: μm).

	At rest		During avascularization	
	Average	SD	Average	SD
Proposed	8.1	2.9	15.2	2.8
Conventional	25.1	7.2	59	0

Table III. RMSEs of fitting (unit: dB).

	At rest	During avascularization
Proposed	0.7	0.3
Conventional	1.5	0.8

averaging the scattering power spectra. These results show that the proposed method will be useful for the accurate evaluation of the degree of RBC aggregation.

4. Conclusions

In the present paper, a method for estimating the size of RBC aggregates without using the power spectrum of the rear wall was proposed by introducing a reference scattering power spectrum calculated by the power spectrum measured for ultrafine wires with a hemispherical tip. The size of the microparticles simulating the RBC aggregates was estimated using the reference scattering power spectra calculated from the power spectrum measured for the ultrafine wire. As a

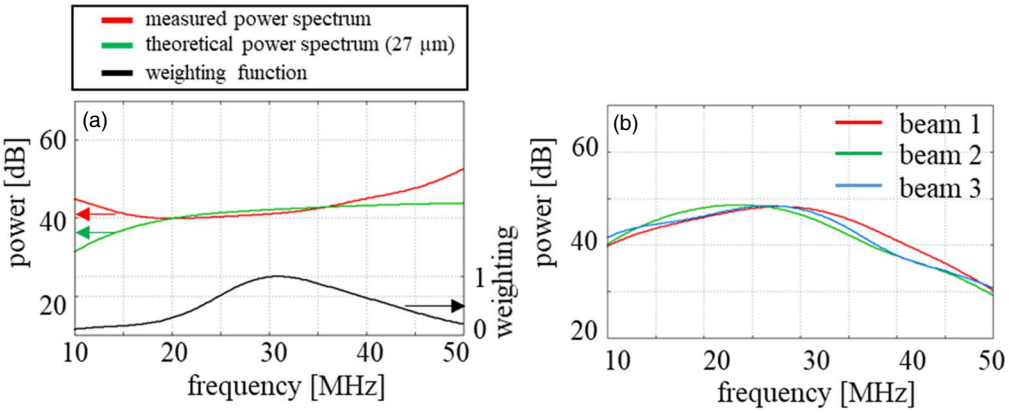

Fig. 9. (Color online) (a) Fitting results by the conventional method, and (b) power spectra of posterior wall which were used for the size estimation by the conventional method.

result, the estimated size was close to the true value, and it shows that the reference power spectra are useful for accurate size estimation of the scatterer sizes. Moreover, the proposed method was applied to in vivo measurements. The estimated size at rest was similar to the size of a single RBC and increased when the RBCs were aggregated by avascularization.

Wires with a hemispherical tip were used for the measurements, but the theoretical model assumed the object to be a sphere. It is necessary to clarify the effect of the deviation of the model on the size estimation. However, the results of this paper show that the proposed method will be useful for accurate size estimation of RBC aggregates.

Acknowledgments

This work was partially supported by JSPS KAKENHI 19K22943.

1) R. Fåhraeus, Physiol. Rev. **9**, 241 (1929).
2) S. Chien and K. Jan, Microvasc. Res. **5**, 155 (1973).
3) S. Chien and L. A. Sung, Clin. Hemorheol. Microcirc. **7**, 71 (1987).
4) O. K. Baskurt, A. Temiz, and H. J. Meiselman, J. Lab. Clin. Med. **130**, 183 (1997).
5) G. Cloutier, A. Zimmer, F. T. Yu, and J. L. Chiasson, Diabetes Care **31**, 1400 (2008).
6) F. T. Yu, J. K. Armstrong, J. Tripette, H. J. Meiselman, and G. Cloutier, J. Thromb. Haemost. **9**, 481 (2011).
7) O. K. Baskurt, A. Herbert, and J. Meiselman, Microcirculation **15**, 585 (2008).
8) J. J. Bishop, P. R. Nance, A. S. Popel, M. Intaglietta, and P. C. Johnson, Am. J. Physiol. Heart Circ. Physiol. **280**, H222 (2001).
9) J. W. Weisel and R. I. Litvinov, J. Thromb. Haemost. **17**, 271 (2018).
10) D. G. Paeng, K. H. Nam, and K. K. Shung, Ultrasound Med. Biol. **36**, 1118 (2010).
11) D. G. Paeng, K. H. Nam, M. J. Choi, and K. K. Shung, IEEE Trans. Ultrason. Ferroelectr. Freq. Control **56**, 880 (2009).
12) S. Beppu, Y. Nimura, H. Sakakibara, S. Nagata, Y. D. Park, and S. Izumi, J. Am. Coll. Cardiol. **6**, 744 (1985).
13) S. Turhan, O. U. Ozcan, and C. Erol, Cor et Vasa **55**, 176 (2013).
14) D. G. Paeng, R. Y. Chiao, and K. K. Shung, Ultrasound Med. Biol. **30**, 45 (2003).
15) D. G. Paeng, R. Y. Chiao, and K. K. Shung, Ultrasound Med. Biol. **30**, 815 (2004).
16) R. L. Callé, F. Ossant, Y. Gruel, P. Lermusiaux, and F. Patat, Ultrasound Med. Biol. **34**, 252 (2008).
17) R. Callé, C. Plag, F. Patat, and F. Ossant, J. Acoust. Soc. Am. **125**, 530 (2009).
18) D. Nicholas, Ultrasound Med. Biol. **8**, 17 (1982).
19) T. Oguri, M. Omura, W. Saito, K. Yoshida, and T. Yamaguchi, Jpn. J. Appl. Phys. **60**, SDDE24 (2021).
20) T. Oguri, K. Tamura, K. Yoshida, J. Mamou, H. Hasegawa, H. Maruyama, H. Hachiya, and T. Yamaguchi, Jpn. J. Appl. Phys. **54**, 07HF14 (2015).
21) T. M. Bui, A. Coron, J. Mamou, E. Saegusa-Beecroft, T. Yamaguchi, E. Yanagihara, J. Machi, S. L. Bridal, and E. J. Feleppa., IEEE Trans. Biomed. Eng. **64**, 1579 (2017).
22) M. Omura, K. Yoshida, S. Akita, and T. Yamaguchi, Jpn. J. Appl. Phys. **59**, SKKE15 (2020).
23) M. Omura, K. Yoshida, S. Akita, and T. Yamaguchi, J. Med. Ultrason. **47**, 25 (2020).
24) E. Franceschini, F. T. H. Yu, and G. Cloutier, J. Acoust. Soc. Am. **123**, EL85 (2008).
25) E. Franceschini, F. T. H. Yu, F. Destrempes, and G. Cloutier, J. Acoust. Soc. Am. **127**, 1104 (2010).
26) R. K. Saha, E. Franceschini, and G. Cloutier, J. Acoust. Soc. Am. **129**, 2269 (2011).
27) B. Chayer, L. Allard, Z. Qin, J. Garcia-Duitama, L. Roger, F. Destrempes, J. F. Cailhier, A. Denault, and G. Cloutier, Clin. Hemorheol. Microcirc. **74**, 109 (2020).
28) N. Saitoh, H. Hasegawa, and H. Kanai, Jpn. J. Appl. Phys. **48**, 07GJ08 (2009).
29) T. Fukushima, H. Hasegawa, and H. Kanai, Jpn. J. Appl. Phys. **50**, 07HF02 (2011).
30) Y. Kurokawa, H. Taki, S. Yashiro, K. Nagasawa, Y. Ishigaki, and H. Kanai, Jpn. J. Appl. Phys. **55**, 07KF12 (2016).
31) M. Arakawa, K. Nagasawa, A. Fukase, K. Higashiyama, S. Mori, S. Yashiro, Y. Ishigaki, and H. Kanai, Proc. IEEE Int. Ultrason. Symp., 2020 , p. 1.
32) K. Nagasawa, A. Fukase, S. Mori, M. Arakawa, S. Yashiro, Y. Ishigaki, and H. Kanai, J. Med. Ultrason. **48**, 3 (2021).
33) H. Sakaki, M. Arakawa, S. Yashiro, Y. Todate, Y. ishigaki, and H. Kanai, J. Med. Ultrason. **46**, 3 (2019).
34) M. Arakawa, H. Sakaki, K. Nagasawa, A. Fukase, S. Mori, S. Yashiro, Y. Ishigaki, and H. Kanai, Proc. IEEE Int. Ultrason. Symp., 2018, p. 1.
35) A. Fukase, K. Nagasawa, S. Mori, M. Arakawa, S. Yashiro, Y. Ishigaki, and H. Kanai, IEEE Int. Ultrason. Symp., 2019, p. 45.
36) A. Fukase, K. Higashiyama, S. Mori, M. Arakawa, S. Yashiro, Y. Ishigaki, and H. Kanai, Jpn. J. Appl. Phys. **60**, SDDE08 (2021).
37) K. Higashiyama, S. Mori, M. Arakawa, S. Yashiro, Y. Ishigaki, and H. Kanai, Proc. Symp. Ultrason. Electr. **42**, 3Pa5 (2021).
38) P. M. Morse and H. Feshbach, *Methods of Theoretical Physics* (McGraw-Hill, New York, 1953), p. 1483.
39) Y. Hashimoto, N. Akashi, and J. Kushibiki, Proc. IEICE Tech. Rep., 1997, p. 37.
40) B. I. Raju and M. A. Srinivasan, Ultrasound Med. Biol. **27**, 1543 (2001).
41) B. E. Treeby, E. Z. Zhang, A. S. Thomas, and B. T. Cox, Ultrasound Med. Biol. **37**, 289 (2011).
42) R. Skalak, N. Ozkaya, and T. C. Skalak, Annu. Rev. Fluid Mech. **21**, 167 (1989).
43) M. L. Turgeon, *Clinical Hematology: Theory and Procedures* (Lippincott Williams & Wilkins, Pennsylvania, 2005), p. 100.